

28. Funabashi, Y., Ohtsubo, K., Eto, M. & Kawamura, K. Phase relaxation and non-equilibrium transport properties through multilevel quantum dot. *Jpn J. Appl. Phys.* **38**, 388–391 (1999).
29. Wingreen, N. S. & Meir, Y. Anderson model out of equilibrium: Noncrossing-approximation approach to transport through a quantum dot. *Phys. Rev. B* **49**, 11040–11052 (1994).
30. Inoshita, T., Shimizu, A., Kuramoto, Y. & Sakaki, H. Correlated electron transport through a quantum dot: The multiple-level effect. *Phys. Rev. B* **48**, 14725–14728 (1993).

**Acknowledgements**

We thank Yu. V. Nazarov, K. Majjala, S. M. Cronenwett, J. E. Mooij and Y. Tokura for discussions. We acknowledge financial support from the Specially Promoted Research, Grant-in-Aid for Scientific Research, from the Ministry of Education, Science and Culture in Japan, from the Dutch Organisation for Fundamental Research on Matter (FOM), from the NEDO joint research program, and from the EU via a TMR network.

Correspondence and requests for materials should be addressed to S.D.F. (e-mail: silvano@qt.tn.tudelft.nl).

**Direct observation of the alignment of ferromagnetic spins by antiferromagnetic spins**

**F. Nolting\***, **A. Scholl\***, **J. Stöhr†**, **J. W. Seo‡§**, **J. Fompeyrine§**, **H. Siegwart§**, **J.-P. Locquet§**, **S. Anders\***, **J. Lüning†**, **E. E. Fullerton†**, **M. F. Toney†**, **M. R. Scheinfein||** & **H. A. Padmore\***

\* Advanced Light Source, 1 Cyclotron Road, Lawrence Berkeley National Laboratory, Berkeley, California 94720, USA

† IBM Research Division, Almaden Research Center, 650 Harry Road, San Jose, California 95120, USA

‡ Institute de Physique, University of Neuchâtel, CH-2000 Neuchâtel, Switzerland

§ IBM Research Division, Zürich Research Laboratory, CH-8803 Rüschlikon, Switzerland

|| Department of Physics and Astronomy, Arizona State University, Tempe, Arizona 85287-1504, USA

The arrangement of spins at interfaces in a layered magnetic material often has an important effect on the properties of the material. One example of this is the directional coupling between the spins in an antiferromagnet and those in an adjacent ferromagnet, an effect first discovered<sup>1</sup> in 1956 and referred to as exchange bias. Because of its technological importance for the development of advanced devices such as magnetic read heads<sup>2</sup> and magnetic memory cells<sup>3</sup>, this phenomenon has received much attention<sup>4,5</sup>. Despite extensive studies, however, exchange bias is still poorly understood, largely due to the lack of techniques capable of providing detailed information about the arrangement of magnetic moments near interfaces. Here we present polarization-dependent X-ray magnetic dichroism spectro-microscopy that reveals the micromagnetic structure on both sides of a ferromagnetic–antiferromagnetic interface. Images of thin ferromagnetic Co films grown on antiferromagnetic LaFeO<sub>3</sub> show a direct link between the arrangement of spins in each material. Remanent hysteresis loops, recorded for individual ferromagnetic domains, show a local exchange bias. Our results imply that the alignment of the ferromagnetic spins is determined, domain by domain, by the spin directions in the underlying antiferromagnetic layer.

We investigated a thin Co film on top of a 40 nm LaFeO<sub>3</sub> film grown on SrTiO<sub>3</sub>(001). The sample was prepared in a molecular beam epitaxy system with the LaFeO<sub>3</sub> film grown using a block-by-block growth method<sup>6</sup> at 750 °C under a beam of atomic oxygen and a partial O<sub>2</sub> pressure of 5 × 10<sup>-6</sup> Torr. This method has been shown to yield high-quality epitaxial films<sup>7</sup>. Plan-view electron-diffraction

and conventional transmission electron microscopy (TEM) analysis show that the epitaxial LaFeO<sub>3</sub> film consists of two microscopic crystallographic domains characterized by orientations of the LaFeO<sub>3</sub> c-axis along the [100] and [010] directions in the SrTiO<sub>3</sub> surface plane<sup>8</sup>. The Co film, grown in the form of a stepped wedge, was deposited *in situ* at room temperature and capped with a 1-nm Pt layer to prevent its oxidation. X-ray diffraction analysis of a sample with a Co thickness of 2.5 nm (and a 1-nm Pt cap layer) revealed a polycrystalline Co structure. Kerr measurements showed that the easy magnetization axis of the sample was in-plane with uniaxial symmetry about the surface normal. All measurements reported here were performed on as-grown samples. Because the samples were not set in a magnetic field they did not exhibit a macroscopic exchange bias<sup>4,5</sup>. (For LaFeO<sub>3</sub>, chemical decomposition prevents the use of setting temperatures close to the Néel temperature (740 K) to create large exchange bias. However, low-temperature (390 K) annealing of Co/LaFeO<sub>3</sub> in a 500-Oe applied field is sufficient to produce a macroscopic bias of 0.007 erg cm<sup>-2</sup> at room temperature and 0.1 erg cm<sup>-2</sup> at 4.2 K). Our ability to probe the spatially resolved magnetic configuration allowed us to observe local bias effects, which average to zero macroscopically.

Spectro-microscopy studies were carried out using the PEEM2 facility at the Advanced Light Source in Berkeley<sup>9</sup>. The focused X-rays, whose polarization could be changed from linear to right or left circular<sup>10</sup>, are incident on the sample at an angle of 30° from the surface and form a 30-μm spot. The low-energy secondary photoelectrons from the sample are imaged by an all-electrostatic photoemission electron microscope (PEEM) with magnification onto a phosphor screen that is read by charge-coupled device (CCD) camera. The spatial resolution of PEEM2 is limited by chromatic aberrations to 20 nm. For imaging we exploited several unique spectroscopic capabilities associated with the variable energy and polarization of the X-rays<sup>10</sup>. By tuning the photon energy to either the Fe L-edge, near 710 eV, or the Co L-edge, near 780 eV, we can record separate images of the antiferromagnetic (AFM) LaFeO<sub>3</sub> layer and the ferromagnetic (FM) Co layer. We use linear X-ray

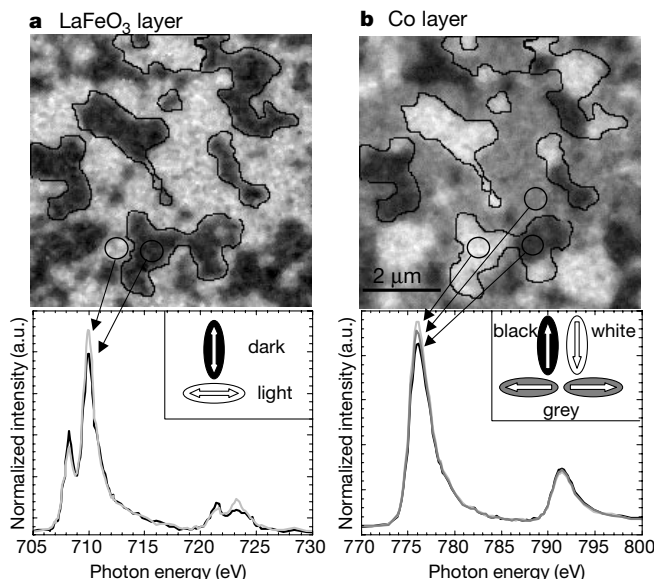


**Figure 1** Images and local spectra from the antiferromagnetic and ferromagnetic layers for 1.2-nm Co on LaFeO<sub>3</sub>/SrTiO<sub>3</sub>(001). **a**, Fe L-edge XMLD image; **b**, Co L-edge XMCD image. The contrast in the images arises from antiferromagnetic domains in LaFeO<sub>3</sub> (**a**) and ferromagnetic domains in Co (**b**) with in-plane orientations of the antiferromagnetic axis and ferromagnetic spins as indicated below the images. The spectra shown underneath were recorded in the indicated areas and illustrate the origin of the intensity contrast in the PEEM images.

polarization to image the microscopic AFM domain structure for LaFeO<sub>3</sub>, making use of the large X-ray magnetic linear dichroism (XMLD) effect associated with the multiplet structure at the Fe L<sub>3</sub> or L<sub>2</sub> edge<sup>8</sup>. In our PEEM geometry the electric field vector **E** is oriented parallel to the surface. We use right- or left-handed circular polarization to image the FM Co domain structure, exploiting the X-ray magnetic circular dichroism (XMCD) effect at the Co L<sub>3</sub> and L<sub>2</sub> edges<sup>11</sup>. In our case, the photon angular momentum was oriented parallel to the X-ray propagation direction, at a 30° angle from the surface. Finally, the relatively short sampling depth (about 2 nm) of the PEEM technique<sup>10</sup> combined with the small thickness of the Co layer allows us to be sensitive to the FM and AFM structure in the vicinity of the interface.

Figure 1 shows images of the domain structure in the AFM LaFeO<sub>3</sub> film and in a 1.2-nm-thick FM Co layer on top of the very same substrate region. The magnetic contrast in the left image arises from AFM domains in LaFeO<sub>3</sub> with an in-plane projection of the AFM axis **A** oriented horizontally (light) and vertically (dark). The four AFM domains in epitaxial LaFeO<sub>3</sub> have their AFM axes tilted by 45° from the surface normal with orthogonal in-plane projections<sup>8</sup>. As in our experimental geometry **E** lies in the surface plane, we cannot distinguish the two domains with collinear in-plane projections and we only observe two of the four AFM domains. Comparison of TEM and PEEM images shows that the AFM domains are seeded by the two epitaxial crystallographic domains<sup>8</sup>. XMLD spectra recorded in the light and dark regions, shown underneath, reveal the spectroscopic origin of the AFM contrast. The FM Co image (Fig. 1b) exhibits three distinct grey scales, corresponding to FM domains aligned vertically up (black) and down (white), and horizontally left or right (grey). For the experimental geometry used for Fig. 1, corresponding to a vertical X-ray propagation direction (and angular momentum), we cannot distinguish left from right horizontally oriented FM domains<sup>10</sup>, but these were resolved by a 90° rotation of the sample (not shown). XMCD spectra recorded for regions with different grey scales (Fig. 1b) illustrate the origin of the intensity contrast. Comparison of the in-plane projections of the

AFM axis and the FM spin directions, illustrated below the images, reveals that the FM Co spins are aligned parallel or antiparallel to the in-plane projection of the AFM axis. The correlation revealed by Fig. 1 is of magnetic rather than crystallographic origin as the Co is polycrystalline. The magnetic alignment of the Co domains, which exhibit an in-plane easy axis, must therefore be caused by a coupling to uncompensated spins at the LaFeO<sub>3</sub> surface with an in-plane component parallel to the in-plane projection of the AFM axis. Experiments that attempted to image the uncompensated Fe spins directly, with XMCD microscopy, were unsuccessful, probably because of their small concentration or magnitude. The uncompensated spins may originate solely from an interface effect as discussed in ref. 12 or from the small parasitic Fe magnetization in LaFeO<sub>3</sub> (ref. 13).

The exchange coupling at the Co/LaFeO<sub>3</sub> interface also causes a local exchange bias in individual Co domains. In Fig. 2a a series of XMCD images demonstrate the magnetization reversal process in the Co layer. The measurements were performed on a 2.5-nm Co/LaFeO<sub>3</sub> sample with the magnetic field applied along the X-ray propagation direction. The microscopic XMCD images were acquired in zero field, because of the strong deflection of the photo-electrons in an applied in-plane field. The images reveal a strong uniaxial anisotropy of the Co domains. Only those Co domains that are coupled to LaFeO<sub>3</sub> domains with the projection of the AFM axis parallel to the field exhibit a magnetization reversal (black to white) while the orthogonal Co domains (grey) follow a hard axis loop and remain unchanged. We furthermore observe a local unidirectional magnetic anisotropy of single Co domains, a local exchange bias. Local remanent hysteresis loops (Fig. 2b), calculated from the field dependent XMCD contrast in a series of images, show a repeatable loop shift up to 30 Oe. This local bias is attributed to a surplus of uncompensated spins in the individual AFM domains which are frozen in after growth. (The dipole fields from the neighbouring Co domains are too small to cause this local bias. Micromagnetic calculations showed that these dipole fields are below 5 Oe for a typical domain pattern (domain size between 0.8 μm<sup>2</sup> and 1.5 μm<sup>2</sup>.) Averaged over the total area shown in Fig. 2a, the bias effects of individual domains cancel out, leading to the unshifted averaged hysteresis loop, also shown in Fig. 2b. The averaged loop exhibits only half of the XMCD brightness change because the orthogonal grey domains constitute half of the signal but do not switch. The lack of bias in the averaged loop is expected, because the studied sample was not set in a magnetic field. The setting procedure would shift the balance of the microscopically biased domains, resulting in a preferred macroscopic spin direction, that is, exchange bias.

Our results open the door for investigations of various ferromagnetic–antiferromagnetic systems consisting of single crystal, polycrystalline or even amorphous materials. As such, they may hold the key to a definitive understanding of the ferromagnetic–antiferromagnetic exchange bias phenomenon. □

Received 10 November 1999; accepted 5 April 2000.

- Meiklejohn, W. H. & Bean, C. P. New magnetic anisotropy. *Phys. Rev.* **102**, 1413–1414 (1956).
- Tsang, C. *et al.* Design, fabrication and testing of spin-valve read heads for high density recording. *IEEE Trans. Mag.* **30**, 3801–3806 (1994).
- Parkin, S. S. P. *et al.* Exchange-biased magnetic tunnel junctions and application to non-volatile magnetic random access memory. *J. Appl. Phys.* **85**, 5828–5833 (1999).
- Nogués, J. & Schuller, I. K. Exchange bias. *J. Magn. Magn. Mater.* **192**, 203–232 (1999).
- Berkowitz, A. E. & Takano, K. Exchange anisotropy—a review. *J. Magn. Magn. Mater.* **200**, 552–570 (1999).
- Locquet, J.-P., Catana, A., Mächler, E., Gerber, C. & Bednorz, J. G. Block-by-block deposition: A new growth method for complex oxide thin films. *Appl. Phys. Lett.* **64**, 372–374 (1994).
- Locquet, J.-P. *et al.* Doubling the critical temperature of La<sub>1-x</sub>Sr<sub>x</sub>CoO<sub>4</sub> using epitaxial strain. *Nature* **394**, 453–456 (1998).
- Scholl, A. *et al.* Observation of antiferromagnetic domains in epitaxial thin films. *Science* **287**, 1014–1016 (2000).
- Anders, S. *et al.* Photoemission electron microscope for the study of magnetic materials. *Rev. Sci. Instrum.* **70**, 3973–3981 (1999).
- Stöhr, J., Padmore, H. A., Anders, S., Stammer, T. & Scheinfein, M. R. Principles of x-ray magnetic dichroism spectromicroscopy. *Surf. Rev. Lett.* **5**, 1297–1308 (1998).

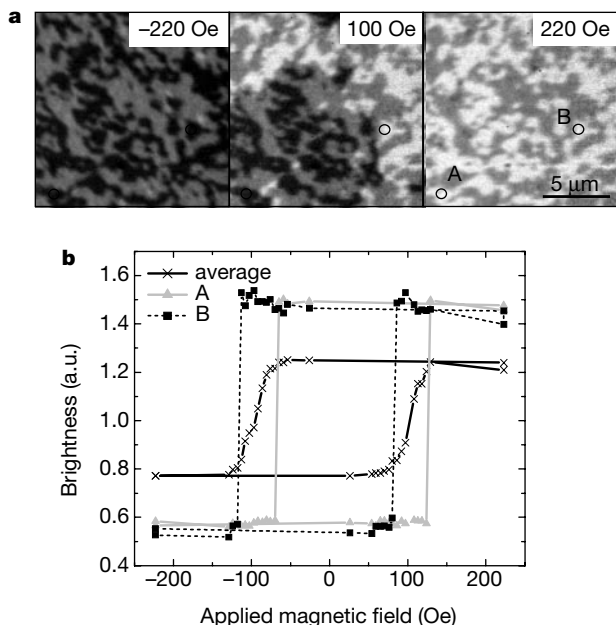


**Figure 2** Field dependence of Co domains for a 2.5-nm Co/LaFeO<sub>3</sub> sample. **a**, Images of the Co domain pattern after applying a magnetic field of -220 Oe, 100 Oe and 220 Oe. The field was applied along the X-ray polarization direction and the images were acquired in zero field. **b**, Local remanent hysteresis loops calculated from the XMCD contrast for two different areas A and B inside domains with the easy axis along the field direction (black and white) and for the entire area in **a**, including grey domains which have their easy axis perpendicular to the field direction.

11. Stöhr, J. *et al.* Element specific magnetic microscopy with circularly polarized X-rays. *Science* **259**, 658–661 (1993).
12. Takano, K. *et al.* Interfacial uncompensated antiferromagnetic spins: role of unidirectional anisotropy in polycrystalline Ni<sub>81</sub>Fe<sub>19</sub>/CoO bilayers. *Phys. Rev. Lett.* **79**, 1130–1133 (1997).
13. Eibschütz, M., Shtrikman, S. & Treves, D. Mössbauer studies of Fe<sup>57</sup> in orthoferrites. *Phys. Rev.* **156**, 562–577 (1967).

**Acknowledgements**

This work was supported by the Director, Office of Basic Energy Sciences, of the US Department of Energy. J.W.S. and E.N. acknowledge support by the Swiss National Science Foundation.

Correspondence and requests for materials should be addressed to E.N. (e-mail: FNolting@lbl.gov).

**Reversible electromechanical characteristics of carbon nanotubes under local-probe manipulation**

Thomas W. Tomblor\*, Chongwu Zhou\*, Leo Alexseyev\*, Jing Kong\*, Hongjie Dai\*, Lei Liu†, C. S. Jayanthi†, Meijie Tang‡ & Shi-Yu Wu†

\* Department of Chemistry, Stanford University, Stanford, California 94305, USA  
 † Department of Physics, University of Louisville, Louisville, Kentucky 40292, USA  
 ‡ Physics Directorate, Lawrence Livermore National Laboratory, Livermore, California 94551, USA

The effects of mechanical deformation on the electrical properties of carbon nanotubes are of interest given the practical potential of nanotubes in electromechanical devices, and they have been studied using both theoretical<sup>1–4</sup> and experimental<sup>5,6</sup> approaches. One recent experiment<sup>6</sup> used the tip of an atomic force microscope (AFM) to manipulate multi-walled nanotubes, revealing that changes in the sample resistance were small unless the nanotubes fractured or the metal–tube contacts were perturbed. But it remains unclear how mechanical deformation affects the intrinsic electrical properties of nanotubes. Here we report an experimental and theoretical elucidation of the electromechanical characteristics of individual single-walled carbon nanotubes (SWNTs) under local-probe manipulation. We use AFM tips to deflect suspended SWNTs reversibly, without changing the contact resistance; *in situ* electrical measurements reveal that the conductance of an SWNT sample can be reduced by two orders of magnitude when deformed by an AFM tip. Our tight-binding simulations indicate that this effect is owing to the formation of local *sp*<sup>3</sup> bonds caused by the mechanical pushing action of the tip.

We prepared samples of individual SWNTs bridging metal electrodes on SiO<sub>2</sub>/Si substrates<sup>7–9</sup>, with part of the SWNT length suspended over trenches fabricated on the SiO<sub>2</sub> surface (Fig. 1a). We characterized the partially suspended individual SWNTs by AFM imaging. Figure 1b shows the AFM image of an SWNT with suspended length *l* ≈ 605 nm over a trench. The image was obtained by tapping-mode AFM (TM-AFM) with the tip scanning direction parallel to the tube axis. Figure 1c shows the experimental setup for bending a suspended SWNT mechanically with an AFM tip while measuring the nanotube electrical properties.

After a desired SWNT device was located and imaged by TM-AFM, the AFM tip was positioned above the centre of the suspended nanotube. The nanotube suspension was pushed towards the bottom of the trench by moving the sample-stage upward. The stage was then retracted. The pushing–retracting cycle was repeated

many times, during which the AFM cantilever deflection and the resistance of the SWNT sample were simultaneously recorded as a function of time. This approach allowed repeated measurements of resistance versus nanotube deflection, as the cantilever deflection signal ( $\Delta Z_c$ ) can readily be converted into the deflection of the suspended nanotube at its centre point ( $\Delta Z_T$ , Fig. 1c). By controlling the initial tip–tube distance  $Z_0$  and the total sample-stage travel range ( $Z_{range}$ ), we were able to deflect the suspended SWNT to various degrees and study the effect of mechanical deformation on the electrical properties of SWNTs.

Figure 2 shows cantilever deflection  $\Delta Z_c$  versus vertical coordinate  $Z$  recorded during one cycle of pushing on the suspended SWNT sample shown in Fig. 1b. Beyond the tip–tube contact point  $Z_0 \approx 50$  nm, the vertical deflection occurring at the centre of the suspended SWNT is  $\delta(Z) = \Delta Z_T(Z) = (Z - Z_0) - \Delta Z_c(Z)$ , and the force applied to the nanotube is  $F(\delta) = k_c \Delta Z_c(\delta)$ . We find that the force  $F(\delta)$  versus nanotube deflection  $\delta$  curve (Fig. 2, inset) right after the tube–tip contact can be fitted well into  $F(\delta) = 8YA(\delta/l)^3$ ,

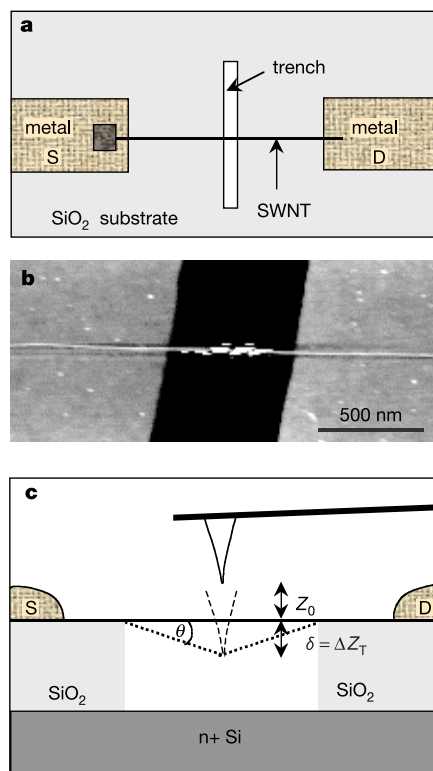


**Figure 1** An SWNT partly suspended over a trench for electromechanical measurements. **a**, Device viewed from above. Preparation of samples involves chemical vapour deposition of SWNTs at desired surface sites using SiO<sub>2</sub>/Si substrates with patterned catalyst islands<sup>7–9</sup>. The substrates contain trenches that are about 500 nm wide and 175 nm deep, pre-fabricated next to patterned catalyst islands (dark square). Thus, the SWNT bridging a pair of metal electrodes (S is the source, D is the drain) is partly suspended over the trench. The spacing between metal electrodes is about 3–4 μm. The metal used to contact SWNTs is 20 nm thick Ti and 60 nm Au placed on top of the SWNTs over a contact length of about 1 μm. **b**, AFM image of an SWNT with suspended length *l* ≈ 605 nm. The cantilever employed for this experiment has a spring constant  $k_c = 0.6$  N m<sup>-1</sup>. The integrated tip on the cantilever is pyramidal with tip radius of about 10–15 nm. The bright streaks around the suspended tube are caused by tube touching and sticking to the side of the pyramid when the tip is scanned near the tube. The diameter of the SWNT  $d = 3.1 \pm 0.2$  nm, measured from the apparent height of the nanotube resting on the SiO<sub>2</sub> surface. The nanotube is a relatively large diameter SWNT synthesized by our chemical vapour deposition approach<sup>7</sup>. It could also be a small SWNT bundle, but this should not change our main conclusions. **c**, Side-view of the AFM pushing experiment. The tip is centred above the SWNT suspension by slowly zooming into the tube-suspension during real-space imaging.

